Received: 6 November 2021 | Accepted: 29 November 2021

DOI: 10.1002/prp2.905

ORIGINAL ARTICLE

Anticancer effects of myricetin derivatives in non-small cell lung cancer in vitro and in vivo

Mengmeng Li | Genlan Zha | Rujun Chen | Xin Chen | Qian Sun | Hao Jiang

Department of Radiation Oncology, The First Affiliated Hospital of Bengbu Medical College, Bengbu, China

Correspondence
Qian Sun and Hao Jiang, Department of Radiation Oncology, The First Affiliated Hospital of Bengbu Medical College, Bengbu, China.
Email: jianghao1223@163.com; sunqianby@163.com

Funding information
This work was supported by the Bengbu City—Bengbu Medical College Joint Science and Technology Project (BYLK201805) and Natural Science Research Project of Bengbu Medical College (BYKY1793).

Abstract

Lung cancer is the most common cause of cancer-related deaths. Moreover, exploring efficient tumor-killing drugs is urgently needed. In our study, several derivative compounds of myricetin were synthesized and tested. Experiments on non-small cell lung cancer (NSCLC) showed that S4-2-2 (5,7-dimethoxy-3-(4-(methyl(1-(naphthalen-2-ylsulfonyl)piperidin-4-yl)amino)butoxy)-2-(3,4,5-trimethoxyphenyl)-4*H*-chromen-4-one) had the strongest effect on A549 cell inhibition across all compounds. Furthermore, S4-2-2-treated A549 cells were also suppressed when transplanted into immunodeficient mice. Particularly, we found that the migration and invasiveness of A549 cells became suppressed upon treatment with S4-2-2. Furthermore, the compound significantly induced cell apoptosis, but did not affect the cell cycle of A549 cells. Finally, we revealed that S4-2-2 inhibited the biological function of NSCLC cells by regulating the protein process in the endoplasmic reticulum, and then by inducing the expression of apoptosis-related proteins. Taken together, S4-2-2 was shown to act as a potential molecular inhibitor of A549 cells.

KEYWORDS
chemotherapy, DNA-damage-inducible transcript 3, endoplasmic reticulum stress, myricetin, non-small cell lung cancer

1 | INTRODUCTION

Lung cancer is a global health concern that has a substantial and increasing burden, as measured by incidence, mortality, and economic cost.[1] In 2019, approximately 228 150 new lung cancer cases have been diagnosed worldwide. Approximately 85% of the diagnoses are non-small cell lung cancer (NSCLC).[2,3] Currently, targeted therapy and immunotherapy are recommended as therapeutic regimens for NSCLC harboring activating mutation(s) and/or biomarker(s), respectively.[4,5] However, the role of traditional chemotherapy in the treatment of NSCLC cannot be ignored in cases where (1) patients are unsuitable for targeted therapy and immunotherapy,[6] (2) patients experience drug resistance after targeted therapy and immunotherapy,[7] and (3) providing an alternative therapeutic option that combines targeted immunotherapy with conventional therapy is necessary.[8] Thus,

Abbreviations: ANOVA, analysis of variance; BSA, bovine serum albumin; FBS, fetal bovine serum; GO, Gene Ontology; KEGG, Kyoto Encyclopedia of Genes and Genomes; NSCLC, non-small cell lung cancer; SD, standard deviation; UPR, unfolded protein response.

Mengmeng Li and Genlan Zha contributed equally to this work and should be considered co-first authors.

screening conventional drugs with tumor sensitivity is important in the treatment of NSCLC.

Natural compounds have long been a source of and/or are complementary to current chemotherapeutic drugs. Natural products and their derivatives contribute to approximately 63% of new drug development.[9] Many studies have shown that myricetin, a flavonoid widely found in tea, fruits, and herbs, has antiproliferative effects on various cancers.[10–12] Shih et al. found that the invasion and migration ability of A549 cells could be suppressed by blocking the extracellular regulated protein kinases signaling pathway.[13] As an attractive candidate, myricetin can inhibit the lung metastasis of breast cancer 4T1 cells in mice.[14] Moreover, myricetin can reportedly act as a radiosensitizer and reduce the survival and proliferation of A549 and H1299 cells compared to radiotherapy alone.[15] Overall, the development of novel myricetin derivatives and the discovery of their tumor-inhibiting activities are critical and confer more options during myricetin-based chemotherapy.

2 | MATERIALS AND METHODS

2.1 | Preparation of S4 series compounds

The four compounds in the S4 series were derived from myricetin synthesized by our team. The molecular weights of the four derivatives, S4-2-2, S4-2-6, S4-2-8, and S4-2-9 were 746.87, 741.81, 697.80, and 747.86, respectively. The following steps have been used to synthesize the derivatives: (a) protect the hydroxyl group of myricitrin with methyl iodide; (b) expose the three hydroxyl groups; (c) synthesize 1,4-dibromobutane; (d) replace the terminal bromine with 1-Boc-4-methylaminopiperidine; (e) remove Boc; and (f) react with sulfonyl chloride to obtain compounds. The derivatives were dissolved in DMSO, and their chemical structures are shown in Figure 1. All four molecules analytical information including mass spectrometry analysis are listed in Tables S1 and S2.

2.2 | Cell culture

The human lung adenocarcinoma cell line A549 was obtained from the Cell Line Bank, Chinese Academy of Science. DMEM (HyClone) containing 10% fetal bovine serum (FBS) (HyClone) was used to culture the cells under 5% carbon dioxide at 37°C. When the cells grew to a density of 80%–90%, they were passaged, and the logarithmic growth cells were harvested for the experiments.

2.3 | MTT assay

An MTT kit (Sigma) was used to measure the cell survival rate in in vitro cytotoxicity tests of the four derivatives. A 96-well plate was used to incubate A549 cells with a density of 3×10^4 cells/

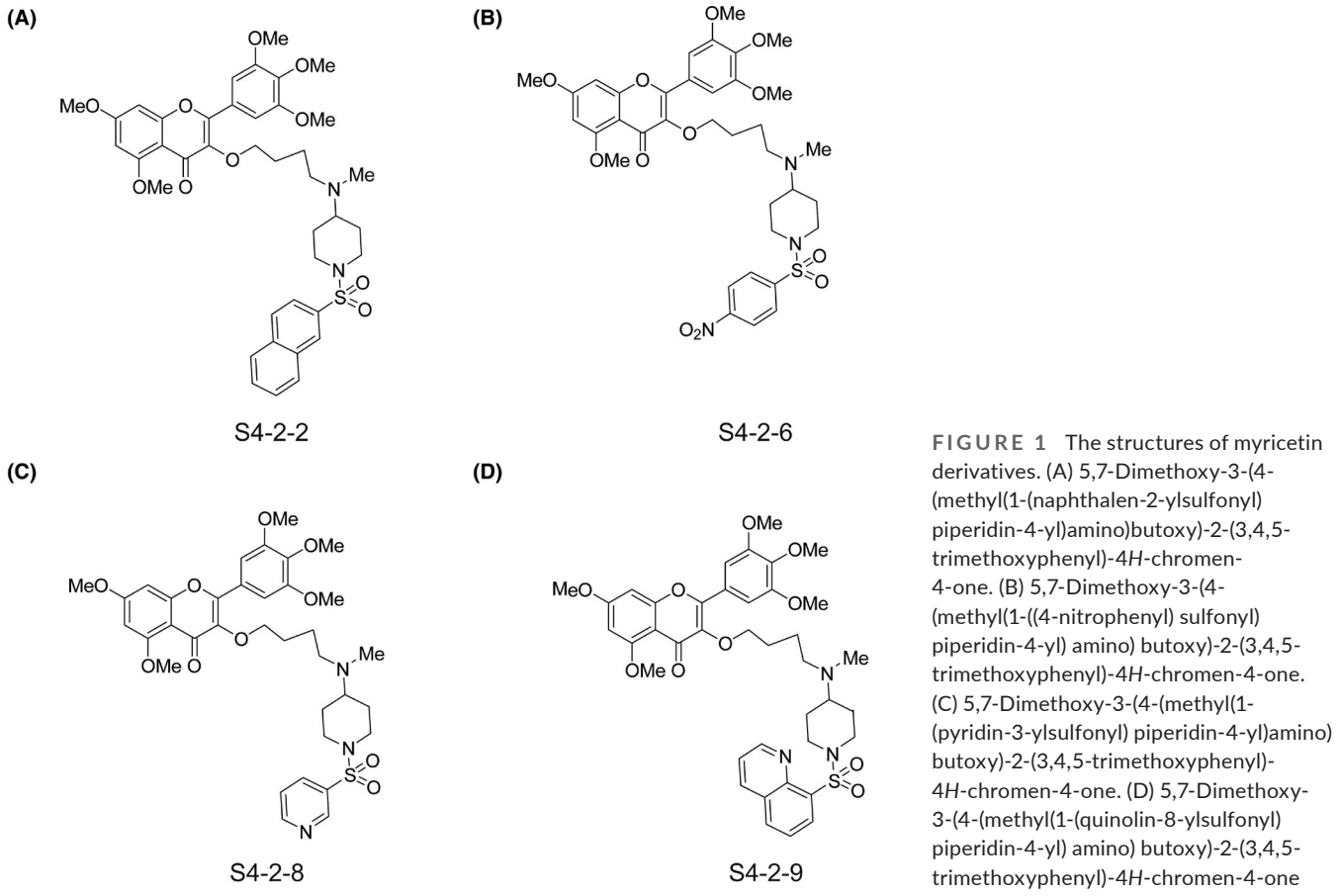

FIGURE 1 The structures of myricetin derivatives. (A) 5,7-Dimethoxy-3-(4-(methyl(1-(naphthalen-2-ylsulfonyl) piperidin-4-yl)amino)butoxy)-2-(3,4,5-trimethoxyphenyl)-4*H*-chromen-4-one. (B) 5,7-Dimethoxy-3-(4-(methyl(1-((4-nitrophenyl) sulfonyl) piperidin-4-yl) amino) butoxy)-2-(3,4,5-trimethoxyphenyl)-4*H*-chromen-4-one. (C) 5,7-Dimethoxy-3-(4-(methyl(1-(pyridin-3-ylsulfonyl) piperidin-4-yl)amino) butoxy)-2-(3,4,5-trimethoxyphenyl)-4*H*-chromen-4-one. (D) 5,7-Dimethoxy-3-(4-(methyl(1-(quinolin-8-ylsulfonyl) piperidin-4-yl) amino) butoxy)-2-(3,4,5-trimethoxyphenyl)-4*H*-chromen-4-one

ml at 37°C for 12 h. Treatment with S4-2-2, S4-2-6, S4-2-8, and S4-2-9 at a final concentration of 10 μM was first performed for 24 h. DMSO was used as the negative control and six replicates were performed for each objective. Subsequently, an MTT assay was performed. MTT, which was dissolved in PBS, was added to the plates, and all cells were cultured for 4 h at 37°C. Next, 100 μl SDS-HCl was used to incubate A549 cells. After the plates were shaken on the oscillator for 10 min, the photos were captured at 24 and 48 h. A Multiskan Ascent spectrophotometer (Thermo Fischer) was used to measure the optical density (OD) at a wavelength of 570 nm.

2.4 | CCK8 assay

To examine the effect of S4-2-2 on A549 cells, the viability of A549 cells was evaluated using the CCK8 kit (Beyotime). Cells (4×10^3/ml) were incubated for 24 h after being plated in 96-well plates (six replicates per group). The cells were treated with various concentrations of S4-2-2 (1, 2, 5, 6, 8, and 10 μM) for 24 and 48 h. Then, WST-8 was added to each well at 37°C for 2 h. A microplate reader (Molecular Devices) was used to record the absorbance value (OD) at 450 nm. Cell viability was calculated using the formula: [(ODtest − ODblank)/(ODcontrol − ODblank)] × 100%.

2.5 | Ki67 staining

Ki67 immunofluorescence was performed to detect the effect of 15 h of S4-2-2 (6 μM) and DMSO treatment to the cell proliferation index. Briefly, PBS was used to wash the cells at a density of 2×10^5/ml, and then polyfluoroalkoxy was used to fix the cells for 10 min. The cells were then incubated with 0.1% Triton-X 100 for 10 min. The cells were blocked with 5% bovine serum albumin (BSA) (Sigma) for 1 h and subsequently incubated with anti-Ki67 antibody (Invitrogen, 1: 200) overnight at 4°C. Following washes, goat anti-mouse (Invitrogen, 1: 500) was used as a secondary antibody. Nuclei were counterstained with DAPI (Sigma).

2.6 | Measurement the inhibition of S4-2-2 in a mouse subcutaneous tumor model

Twelve healthy immuno-deficient mice have been skinned on their right hips and received 1×10^7 A549 cells per mouse through subcutaneous injection.

Twelve tumor-bearing mice were randomly divided into two groups to receive DMSO and S4-2-2 (50 μl of 6 μM S4-2-2 each mouse) injection twice on the 5th and 10th days after tumor transplantation. We measured the tumor length (L) and tumor width (W) every 2 days and calculated the tumor weight at the end of the experiment. Tumor volume was calculated as follows: Vn (mm^3) = leng th * width * width/2.

2.7 | HE staining and TUNEL staining

The tumors harvested from the tumor-bearing mice were fixed with 4% paraformaldehyde, and then the tumor sections were embedded in paraffin. To examine the tumor burden, hematoxylin and eosin (HE) (Solarbio) was used to stain some of the tumor sections, whereas some of the sections were subjected to TUNEL staining to detect apoptosis. For the TUNEL-staining assay, proteinase K was used to treat all sections for 15 min at room temperature. The sections were further stained with a TdT-mediated dUTP Nickel End Labelling Kit (Beyotime).

2.8 | Transwell assay

A transwell assay kit (BD Biosciences) was used to measure cell invasion. A Matrigel of 5 mg/L was coated on the upper surface of the basement membrane of the transwell chambers. After air-drying at room temperature, the basement membrane was hydrated with a serum-free culture solution of 1% BSA (Sigma), and the upper layer was inoculated with cells (1×10^5/ml). DMEM containing 5% FBS was added to the lower layer. After culturing with DMSO or the drugs at 1, 6, and 10 μM for 24 h, cotton swabs erased the upper layer cells and 4% paraformaldehyde fixed the lower layer cells for HE staining.

2.9 | Scratch wound healing assay

A549 cells (2×10^5/ml) were inoculated into a 6-well plate, and a scratch was made on the cell layer using 200-μl pipette tips after the cells grew to confluence. DMEM containing 1% FBS was used to culture the cells. Images were captured under an inverted microscope at 0, 12, 24, and 48 h. Eight views were captured for each group. The healing area of the scratch wound was calculated using ImageJ software through the formula Healing area% = (Test scratch area/0 h scratch area) × 100%.

2.10 | Cell apoptosis

Apoptosis was assayed using a cell apoptosis kit (Beyotime). A549 cells with a density of 1×10^6/ml, which have been cultured in the logarithmic growth phase, were seeded into a 6-well plate. After 6 μM of S4-2-2 was added to the medium for another 15 h, the cells were harvested and suspended in a solution containing 5 μl Annexin V-FITC and 10 μl PI, and were incubated at 37°C for 15 min. Cells that received the same volume of DMSO were used as the control group. Apoptosis was immediately detected using a flow cytometer (Beckman Coulter).

2.11 | Cell cycle

The cell cycle was assayed using a cell cycle kit (Beyotime) according to the manufacturer's guidelines. A549 cells with a density of

1×10^6/ml, which have been cultured in the logarithmic growth phase, were seeded into a 6-well plate. To synchronize the cell cycle, the cells were cultured in serum-free medium for 12 h after 24 h of culture in a normal medium. Then, the cells were cultured for 15 h with 6 μM S4-2-2 in a normal medium. Next, the cells were harvested and fixed on ice with pre-chilled 70% ethanol for 4 h. A549 cells were re-suspended in 500 μl PI staining buffer containing 10 μl LRNaseA and 10 μl propidium bromide, and incubated in the dark at 37°C for 30 min. Finally, the cells were analyzed using a flow cytometer (Beckman Coulter) after being passed through a nylon filter.

2.12 | RNA sequencing

Transcription analysis of A549 cells was performed through whole-genome RNA sequencing. Cells were incubated in 6 μM of S4-2-2 for 15 h, and then the TRIzol rea-gent (Thermo Fisher) was used to isolate the total RNA according to the manufacturer's instructions. The RNA concentration was measured using Qubit (Life Technologies), and sequencing and data analysis were performed by Shanghai Liebing Co., Ltd.

2.13 | Real-time PCR

The gene expression of four genes selected from RNA sequencing and related publications was examined by RT-PCR. A549 cells were treated with 6 μM of S4-2-2 or DMSO for 15 h, and total mRNA was isolated with TRIzol according to a standard protocol. An m-MLV reverse transcriptase kit (Bioneer Co.) was used to synthesize cDNA from 2 μg of mRNA. The sequences of the primers for the genes are listed in Table S3, and the human GAPDH gene was used as an internal control.

2.14 | Western blot

A549 cells were treated with 6 μM S4-2-2 and DMSO for 24 h. RIPA buffer (Cell Signaling Technology) was used to extract total proteins. A Pierce™ BCA Protein Assay Kit (23227, Thermo Scientific) was used to quantify protein concentration. The 10% SDS-PAGE gel was used to load and separate 30 μg of protein from each sample at 80–120 V. Then, the protein was transferred to nitro-cellulose for 2 h at a current of 200 mA. After blocking for 1 h with 5% milk, the membranes were incubated with primary antibodies (anti-Bax, Proteintech, 50599-2-ig, 1: 500; anti-P53, Proteintech, 10442-1-AP; 1: 500; anti-Caspase-3, Proteintech, 19677-1-AP, 1: 500; anti-Bcl2, Proteintech, 26593-1-AP, 1: 500; and anti-β-actin, a mouse antibody, BOSTER, BM0627, 1:500, which was set as an internal control) for 12 h at 4°C. This was followed by incubation with the corresponding secondary antibodies (goat anti-rabbit IgG, Proteintech, 15015, 1: 10 000) and goat anti-mouse IgG (Invitrogen, A28177, 1: 10 000) conjugated to horseradish peroxidase. The signal was developed with a horseradish peroxidase developer solution and visualized using a Bio-Rad. The gray value of each band was quantified using ImageJ software. Each sample was analyzed in triplicate.

2.15 | Statistical analysis

The data were statistically analyzed using SPSS 21.0, and the data are presented as the mean ± standard deviation (SD). One-way analysis of variance (ANOVA) was used for statistical analysis, followed by Tukey's post-hoc test. Statistical significance was set at $p < .05$.

3 | RESULTS

3.1 | S4-2-2 significantly suppressed A549 cell proliferation

We focused on myricetin and synthesized its derivatives, termed S4-2-2, S4-2-6, S4-2-8, and S4-2-9. These synthesized compounds had variable inhibitory effects on A549 cells (78.2 ± 8.1%, 22.6 ± 9.1%, 21.1 ± 7.0%, and 58 ± 7.0%, respectively) and S4-2-2 had the strongest inhibitory effect on tumor cells (Figure 2A,B). The CCK8 assay was performed and the results showed that S4-2-2 could suppress cell proliferation in a dose-dependent manner, and the IC50 at 24 and 48 h were 6.38 and 3.25 μM, respectively (Figure 2C). Ki67 staining also showed that S4-2-2 significantly inhibited the proliferation of A549 cells (Figure 2D–F).

3.2 | S4-2-2 inhibits the growth of A549 cell xenografts

The xenografts have been created by transplanting A549 cells into immunodeficient mice, which were then randomly divided into two groups and treated with either DMSO or S4-2-2. In the S4-2-2 administration group, the tumor volume inhibition rate was 41.9% and the tumor weight was significantly attenuated than the DMSO group (DMSO: 1.16 ± 0.1 g; S4-2-2: 0.96 ± 0.1 g, Figure 3A,B). Furthermore, the tumor burden in mice that received S4-2-2 treatment was lower than that in the DMSO control mice (Figure 3C). Conversely, the number of apoptotic cells increased after S4-2-2 treatment (Figure 3D).

3.3 | S4-2-2 significantly attenuated the invasiveness and migration of A549 cells

Cell invasion and migration were detected using the Matrigel-covered transwell assay and wound-healing assay. The transwell assay showed that the invasiveness of A549 cells was inhibited by S4-2-2 in a dose-dependent manner (Figure 4A,B). The wound-healing test also showed that the number of migrating cells was significantly reduced after S4-2-2 treatment (Figure 4C,D).

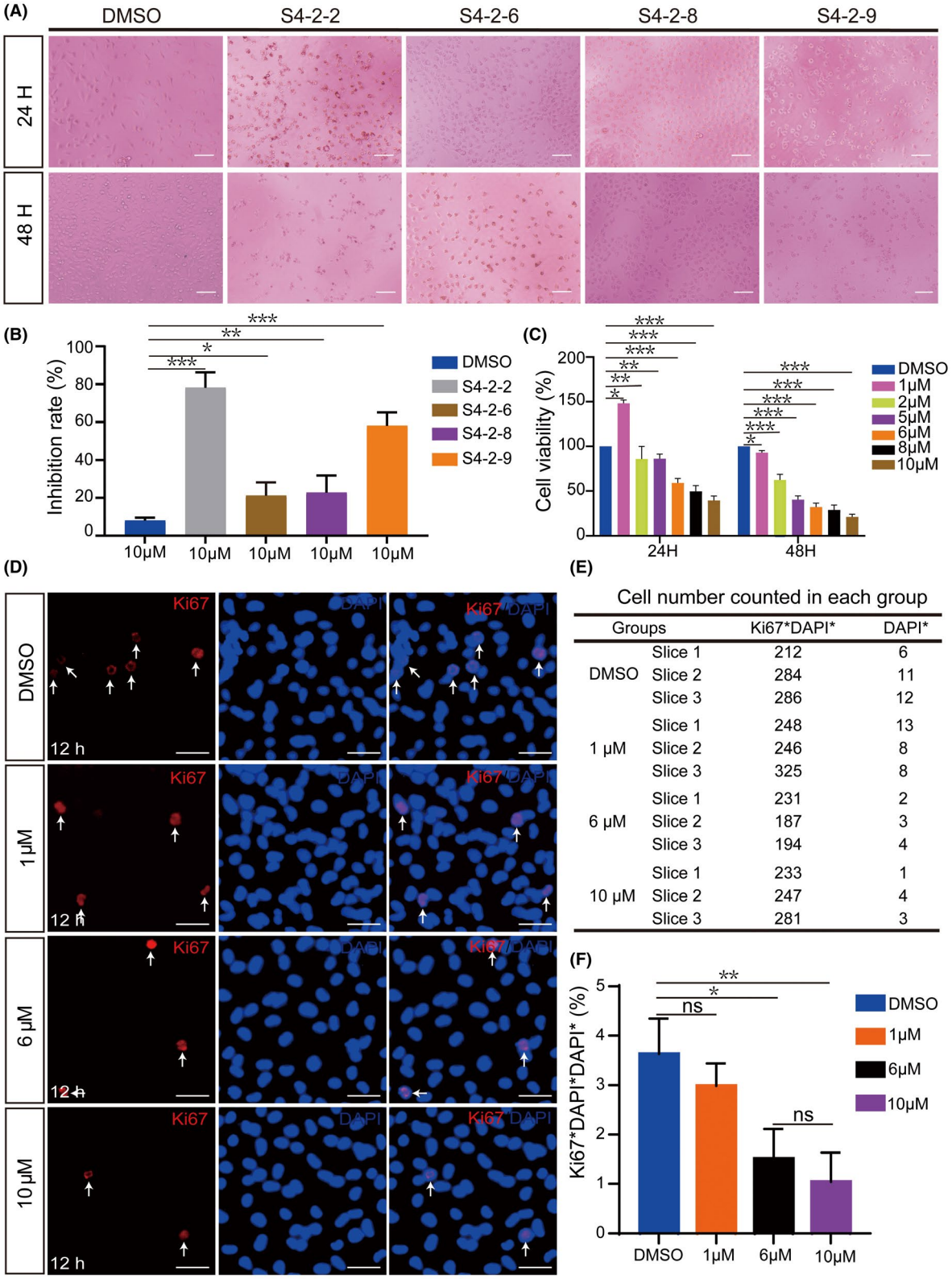

FIGURE 2 S4-2-2 was discovered to significantly suppress A549 cell proliferation in vitro. (A) The bright views of cultured A549 cells treated with DMSO, S4-2-2, S4-2-6, S4-2-8, and S4-2-9 for 24 h (upper) and 48 h (lower), the final concentration was 10 μM. (B) MTT results showed the inhibition rate on A549 cells of each candidate upon 10 μM final concentration. (C) CCK8 results of S4-2-2 on A549 cells. (D) Immunostaining for Ki67 on A549 cells after treating with S4-2-2 for 15 h. (E) The number of counted cells and (F) statistical data of Ki67 + DAPI + cells/DAPI + cells, $n = 3$. The results were presented as means ± SD. The scale bar is 100 μm. $^{*}p < .05$, $^{**}p < .01$, $^{***}p < .001$

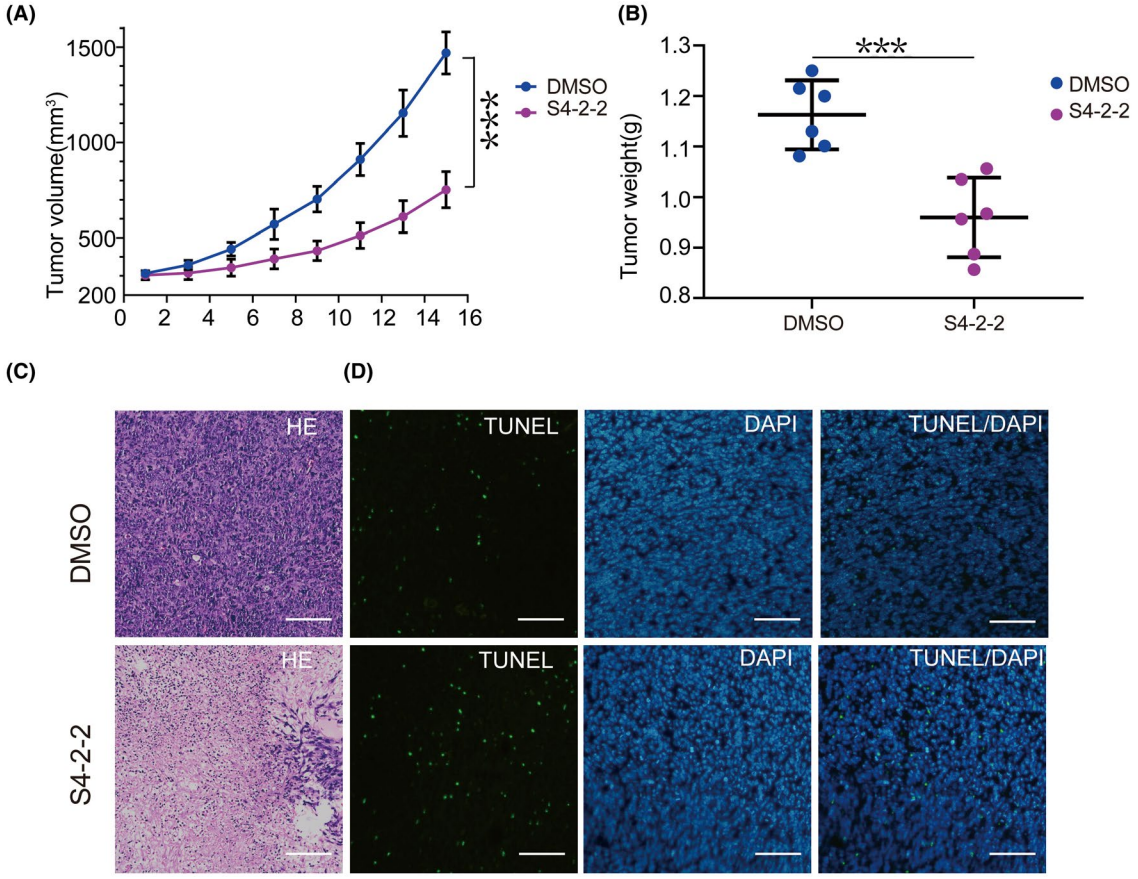

FIGURE 3 S4-2-2 mitigates cell growth and enhances cell apoptosis in xenografts of A549 cells. (A) Tumor volume curves of xenografts after treated with DMSO and S4-2-2 were recorded every 2 days, $n = 6$. (B) Tumor weight of xenografts of A549 cells measured at 15th day between experimental and control groups. $n = 6$. The results are presented as means ± SD. (C) HE staining and (D) Tunel immunohistochemical assay showed the necrosis and apoptosis on slices from xenografts treated with DMSO (upper) and S4-2-2 (bottom), respectively. $n = 6$. The scale bar is 100 μm. $^{***}p < .001$

3.4 | S4-2-2 significantly induced the cell apoptosis of A549 cells, but not the cell cycle

We further examined whether S4-2-2 significantly increased the apoptosis of A549 cells through flow cytometry (DMSO: 7.56% ± 1.44%; S4-2-2: 31.07% ± 4.23%; Figure 5A,B). While we observed that S4-2-2 showed a trend of an increasing number of cells with cell cycle arrest at the G1 phase, the difference was not statistically significant (Figure 5C,D).

3.5 | S4-2-2 suppressed A549 cells by influencing the biological behavior of NSCLC cells through the regulation of endoplasmic reticulum stress and steroid biosynthesis

By comparing the transcriptional profile of A549 cells in the S4-2-2 and DMSO groups treated for 15 h, 860 differentially expressed genes were identified, including 541 upregulated genes and 319 downregulated genes (Figure 6A,B). Furthermore, the details are presented in the supplementary file. The enriched pathways were identified using Gene Ontology (GO) and Kyoto Encyclopedia of Genes and Genomes (KEGG) pathway analysis. Among them, the protein process in the ER pathway was the most significantly activated (Figure 6C). Abnormal protein processing in the ER is highly correlated with ER stress and the unfolded protein response (UPR).[16] The expression of DDIT3, which acts as the effector protein of ER stress,[17] was highly upregulated after 15 h of treatment with S4-2-2 (Figure 6D). In addition, the steroid biosynthesis pathway was also highly activated (Figure 6C), and the transportation of steroids was also enhanced, indicating that STARD4 was in-creased by S4-2-2 stimulation (Figure 6E).[18] Moreover, we observed that some of the apoptotic and anti-apoptotic genes showed a trend of increasing and decreasing expression after 15 h of treatment with S4-2-2 and DMSO, respectively, but this trend was not statistically significant (Figure 6F–H). By contrast, the majority index of increasing A549 cell apoptosis was significantly elevated after 24 h of S4-2-2 treatment (Figure 6I–L). Considering all of these findings, S4-2-2 therefore inhibited the biological behaviors of NSCLC cells by inducing ER disorder, disturbing steroid biosynthesis, and through subsequent apoptosis.

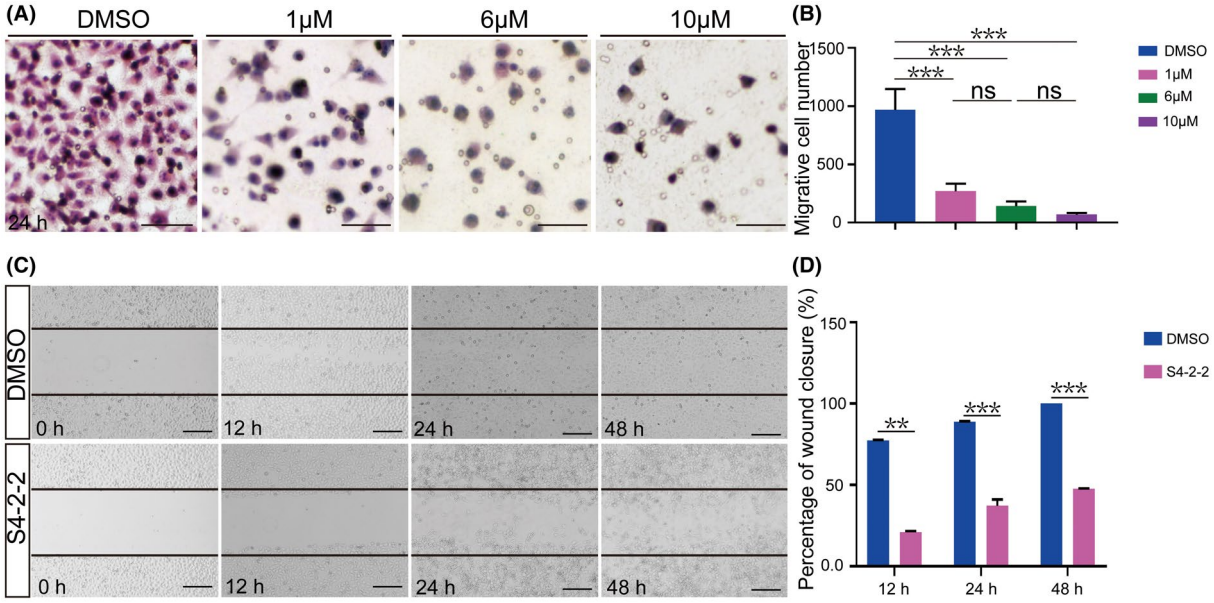

FIGURE 4 S4-2-2 significantly attenuated migration and invasiveness of A549 cells. (A, B) Transwell results showed the effects of S4-2-2 with indicated concentrations on cell migration and invasiveness of A549 cells at 24 h. (C, D) Measuring the inhibition of S4-2-2 upon 6 μM on cell migration of A549 cells at 0, 12, 24, and 48 h by the wound healing assay. The results are presented as means ± SD. The scale bar is 100 μm. $^{**}p < .01$, $^{***}p < .001$

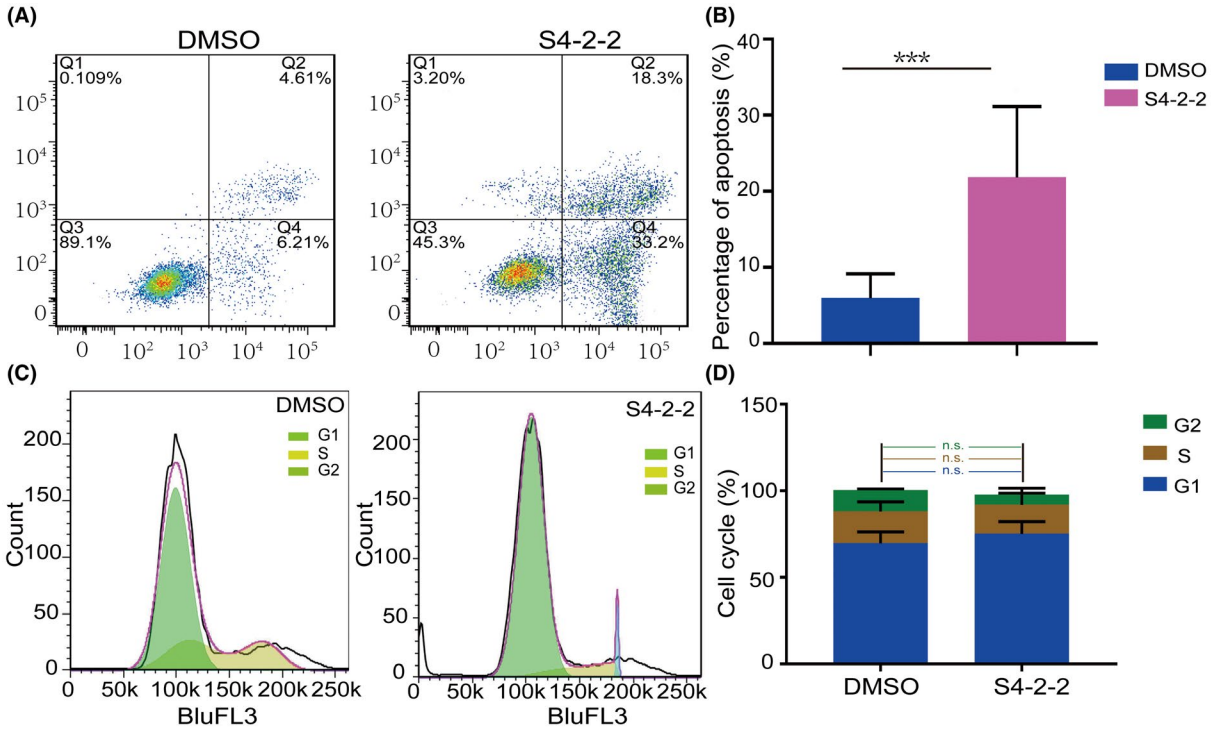

FIGURE 5 S4-2-2 significantly induced A549 cell apoptosis, but not cell cycle. (A) The dot plot of apoptosis of A549 treated with S4-2-2 and DMSO by the flow cytometer. (B) The statistics data showed the ratio of apoptotic cells in early apoptosis, $n = 3$. (C) The flow cytometry curves showed the cell cycle phase of A549 cells incubated with DMSO (left) and S4-2-2 (right). (D) The statistics showed the cell cycle frequency of G1, S, and G2 of A549 cells treated with DMSO and S4-2-2, $n = 3$. The results are presented as means ± SD. A two-tailed *t*-test for group comparison in (B) and (D) $^{***}p < .001$, n.s. refers as no significant

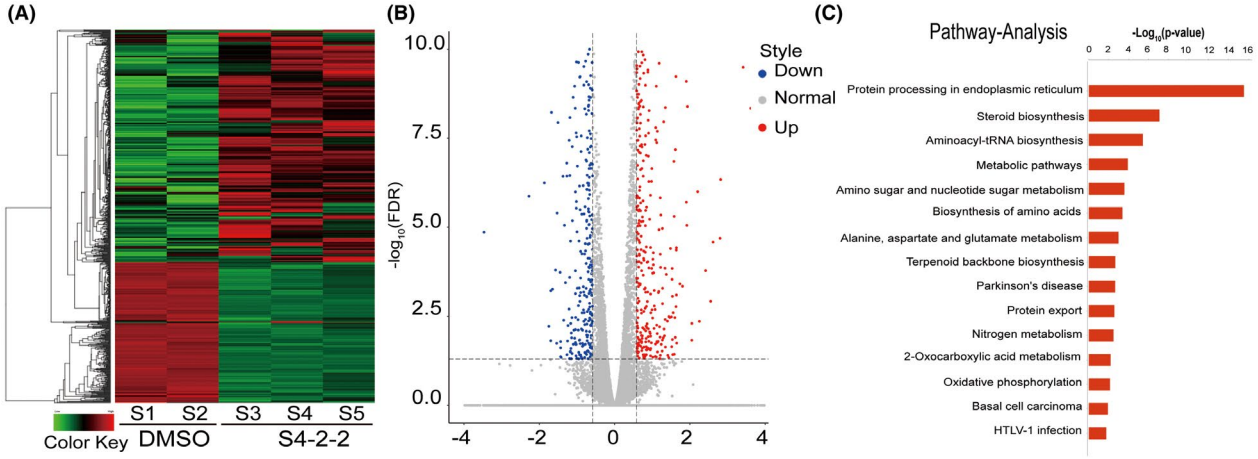

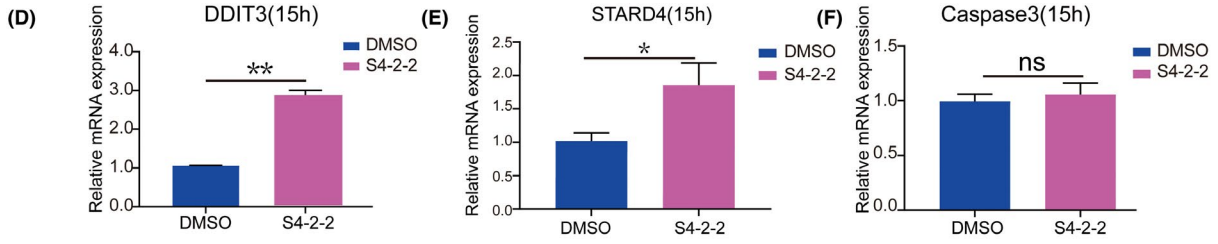

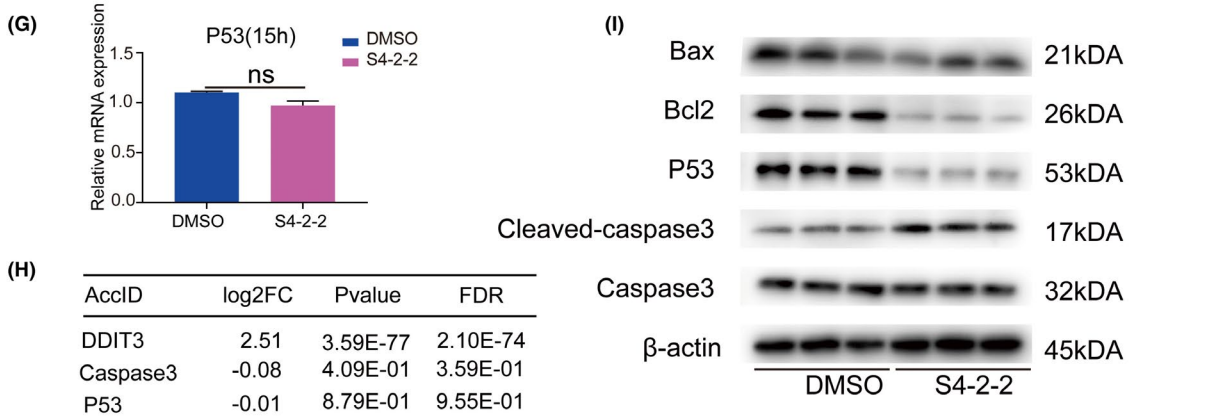

(H)

AccID	log2FC	Pvalue	FDR
DDIT3	2.51	3.59E-77	2.10E-74
Caspase3	-0.08	4.09E-01	3.59E-01
P53	-0.01	8.79E-01	9.55E-01

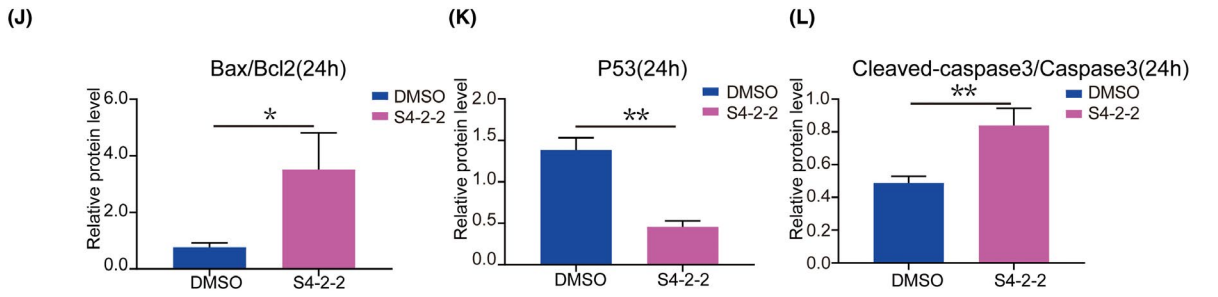

FIGURE 6 The mechanism of action on A549 cells of S4-2-2. (A) Heat map of the top 860 differentially expressed genes (541 upregulated and 319 downregulated genes) by RNA-seq. (B) Volcano plot of the distribution of all differentially expressed genes. (C) Activated pathways of differentially expressed genes by gene ontology analysis. (D) The mRNA expression level of DDIT3 was measured by RT-PCR. (E) The mRNA expression level of STARD4 was measured by RT-PCR. (F) The mRNA expression level of caspase-3 was measured by RT-PCR. (G) The mRNA expression level of P53 was measured by RT-PCR. Six replicates were performed when RT-PCR was carried out. (H) The fold change of DDIT3, caspase-3, and P53 was further analyzed based on the RNA-seq data. (I) The protein level of Bax, Bcl2, P53, caspase-3, and cleaved caspase-3 were measured by western blotting, the cells were harvested at 24 h after S4-2-2 treatment. β-Actin was used as an internal control. (J) The quantification of the ratio of Bcl2/Bax, which represents and negative correlates with the ability of anti-apoptosis. (K) Quantification of the expression level of P53 according to western blotting results. (L) The ratio indicates the apoptosis calculated by gray value (cleaved caspase-3)/gray value (caspase-3). The results are presented as means ± SD. A two-tailed *t*-test was employed in group comparison. $^{*}p < .05$, $^{**}p < .01$, $^{***}p < .001$

4 | DISCUSSION

Chemotherapy during the early stage of NSCLC is still needed in the targeted therapy era.[19] As a natural compound, myricetin exerts antiproliferative and anti-metastatic effects on several tumor cells.[20,21] Here, we focused on the biological functions of four synthesized myricetin derivatives in the regulation of NSCLC. In particular, S4-2-2 was found to exert a relatively higher inhibitory effect on A549 cells (Figure 2A,B). The experimental results showed that the proliferation of A549 cells was mitigated by nearly half at 24 h and was considerably inhibited at 48 h after treatment with S4-2-2 at a concentration of 6 μM (Figure 2C,D). Considering that a higher concentration (i.e., 10 μM) S4-2-2 treatment will inevitably cause catastrophic cell death, we used 6 μM as the final concentration in most of the tests. Xenografts treated with S4-2-2 at 6 μM also showed attenuated growth ability (Figure 3).

Compared with cell proliferation, the cell migration and invasiveness of A549 cells were more sensitive to S4-2-2, as we observed that 1 μM drug administration was sufficient to limit the cellular motor capacity of A549 cells (Figure 4). This capacity endowed S4-2-2 with potential applications in advanced metastatic tumors. Moreover, the in vitro and in vivo results indicated that S4-2-2 induced early- and late-stage cell apoptosis (Figure 5A,B), but did not change the cell cycle of A549 cells (Figure 5C,D).

To elucidate the mechanism underlying the roles of S4-2-2 in NSCLC, a transcriptional sequencing assay was performed. S4-2-2-treated A549 cells and DMSO-treated A549 cells were harvested at 15 h after drug treatment, when the cells showed a significant change in drug-induced cell morphology. We then observed that protein processing in the ER pathway was highly activated in A549 cells after S4-2-2 treatment (Figure 6C). We observed that the proteins in the ER, which is a subcellular organelle, are folded. Misfolded proteins are retained within the ER for ER-associated degradation. In contrast, folded proteins are shuttled into the Golgi complex. The UPR, which includes ER stress and a signaling pathway, is caused by the accumulation of misfolded proteins in the ER, which are induced by harmful endogenous or exogenous stimulation. If ER stress cannot be reversed, it will cause deterioration of cell function and lead to cell death.[22] Enormous data analyses have shown that one of the key pathways to mediate the myricetin inhibition of multiple tumors is ER stress.[23,24]

Mitochondrial apoptosis, which occurs in a variety of cells, is induced by UPR. In mitochondrial apoptosis, the release of cytochrome c is allowed by an outer mitochondrial membrane pore, which is regulated by Bcl2 family proteins. Moreover, an outer mitochondrial membrane pore can also activate caspase-9 in apoptotic bodies, which subsequently activates the apoptotic effector caspase-3 and caspase-7 to induce cell apoptosis.[25] DDIT3 is an ER stress-related gene that also acts as a remote effector to mediate apoptosis.[26,27] After 15 h of S4-2-2 treatment, we detected that the signaling pathway of protein processing in the ER was activated (Figure 6C) and that DDIT3 was highly upregulated in A549 cells (Figure 6D). Enhanced expression of an apoptosis-related gene (Caspase-3) and attenuated expression of anti-apoptotic genes (Bcl2 and P53) were also observed until 24 h after drug administration, followed by ER disorder (Figure 6I–L). These results suggest that S4-2-2 activated ER stress and UPR, and hence induced apoptosis in A549 cells.

Cholesterol, the main component of steroids, is synthesized through multiple steps in most nucleated mammalian cells, mainly in the ER.[28] ER stress can promote cholesterol synthesis and mitochondrial cholesterol influx, leading to cell apoptosis under different stimuli through a complex signaling pathway.[29,30] In this study, we observed that the steroid biosynthesis pathway was activated after S4-2-2 treatment (Figure 6C). Furthermore, cholesterol transportation was also enhanced as STARD4, which participates in the non-cystic transport of cholesterol in the cell,[18] was significantly up-regulated after S4-2-2 treatment (Figure 6E). Nevertheless, the change in steroid levels with S4-2-2 interference and the underlying biological functions require further exploration.

5 | CONCLUSIONS

In summary, we have developed a novel myricetin derivative that functions in NSCLC cell inhibition, and explored a potential complex pathway for this derivative, which regulates the progression of tumor cells.

DISCLOSURE

The authors declare no conflict of interest.

ACKNOWLEDGEMENT

This study was supported by the Bengbu City - Bengbu Medical College Joint Science and Technology Project (BYLK201805) and Natural Science Research Project of Bengbu Medical College (BYKY1793).

AUTHOR CONTRIBUTIONS

Conceptualization: M.L. and G.Z.; methodology: M.L.; software: G.Z.; validation: R.C., M.L. and X.C.; formal analysis: M.L.; resources: H.J.; data curation: Q.S.; writing original draft preparation: M.L.; writing—review and editing: H.J.; supervision: Q.S.; project administration: Q.S.; funding acquisition: H.J. All authors have read and agreed to the published version of the manuscript.

ETHICS STATEMENT

All animal experiments were approved by the Animal Ethical Committee of Bengbu Medical College (No. 2020-185).

INSTITUTIONAL REVIEW BOARD STATEMENT

Not applicable.

INFORMED CONSENT STATEMENT

Not applicable.

DATA AVAILABILITY STATEMENT

The data presented in this study are available on request from the corresponding author.

ORCID

Mengmeng Li https://orcid.org/0000-0002-5876-4682

REFERENCES

1. Feng H, Ge F, Du L, Zhang Z, Liu D. MIR-34B-3P represses cell proliferation, cell cycle progression and cell apoptosis in non-small-cell lung cancer (NSCLC) by targeting CDK4. *J Cell Mol Med*. 2019;23:5282-5291. doi:10.1111/jcmm.14404
2. Herbst RS, Morgensztern D, Boshoff C. The biology and management of non-small cell lung cancer. *Nature*. 2018;553:446-454. doi:10.1038/nature25183
3. Wu Q, Xiong Y, Zhang S, et al. A meta-analysis of the efficacy and toxicity of twice-daily vs. Once-daily concurrent chemoradiotherapy for limited-stage small cell lung cancer based on randomized controlled trials. *Front Oncol*. 2020;9:1454-1460. doi:10.3389/fonc.2019.01460
4. Qiu Z, Chen Z, Zhang C, Zhong W. Achievements and futures of immune checkpoint inhibitors in non-small cell lung cancer. *Exp Hematol Oncol*. 2019;8:19-37. doi:10.1186/s40164-019-0143-z
5. Hirsch FR, Scagliotti GV, Mulshine JL, et al. Lung cancer: current therapies and new targeted treatments. *Lancet*. 2017;389:299-311. doi:10.1016/s0140-6736(16)30958-8
6. Osmani L, Askin F, Gabrielson E, Li QK. Current who guidelines and the critical role of immunohistochemical markers in the subclassification of non-small cell lung carcinoma (NSCLC): moving from targeted therapy to immunotherapy. *Semin Cancer Biol*. 2018;52:103-109. doi:10.1016/j.semcancer.2017.11.019
7. Creelan BC, Gray JE, Tanvetyanon T, et al. Phase 1 trial of dasatinib combined with afatinib for epidermal growth factor receptor-(EGFR-) mutated lung cancer with acquired tyrosine kinase inhibitor (TKI) resistance. *Br J Cancer*. 2019;120:791-796. doi:10.1038/s41416-019-0428-3
8. Sabari JK, Lok BH, Laird JH, Poirier JT, Rudin CM. Unravelling the biology of SCLC: implications for therapy. *Nat Rev Clin Oncol*. 2017;14:549-561. doi:10.1038/nrclinonc.2017.71
9. Chantarawong W, Chamni S, Suwanborirux K, Saito N, Chanvorachote P. 5-O-acetyl-renieramycin T from blue sponge *Xestospongia* sp. induces lung cancer stem cell apoptosis. *Mar Drugs*. 2019;17:19-35. doi:10.3390/md17020109
10. Jiang M, Zhu M, Wang L, Yu S. Anti-tumor effects and associated molecular mechanisms of Myricetin. *Biomed Pharmacother*. 2019;120:109506-109515. doi:10.1016/j.biopha.2019.109506
11. Li M, Chen J, Yu X, et al. Myricetin suppresses the propagation of hepatocellular carcinoma via down-regulating expression of yap. *Cells*. 2019;8:358-373. doi:10.3390/cells8040358
12. Liao HH, Zhang N, Meng YY, et al. Myricetin alleviates pathological cardiac hypertrophy via TRAF6/TAK1/MAPK and NRF2 signaling pathway. *Oxid Med Cell Longev*. 2019;2019:6304058-6304072. doi:10.1155/2019/6304058
13. Shih YW, Wu PF, Lee YC, Shi MD, Chiang TA. Myricetin suppresses invasion and migration of human lung adenocarcinoma A549 cells: possible mediation by blocking the ERK signaling pathway. *J Agric Food Chem*. 2009;57:3490-3499. doi:10.1021/jf900124r
14. Ci Y, Zhang Y, Liu Y, et al. Myricetin suppresses breast cancer metastasis through down-regulating the activity of matrix metalloproteinase (MMP)-2/9. *Phytother Res*. 2018;32:1373-1381. doi:10.1002/ptr.6071
15. Zhang S, Wang L, Liu H, Zhao G, Ming L. Enhancement of recombinant Myricetin on the radiosensitivity of lung cancer A549 and H1299 cells. *Diagn Pathol*. 2014;9:68-74. doi:10.1186/1746-1596-9-68
16. Lin T, Lee JE, Kang JW, Shin HY, Lee JB, Jin DI. Endoplasmic reticulum (ER) stress and unfolded protein response (UPR) in mammalian oocyte maturation and preimplantation embryo development. *Int J Mol Sci*. 2019;20:409-427. doi:10.3390/ijms20020409
17. Kim J, Song H, Heo HR, et al. Cadmium-induced ER stress and inflammation are mediated through C/EBP-DDIT3 signaling in human bronchial epithelial cells. *Exp Mol Med*. 2017;49:372-382. doi:10.1038/emm.2017.125
18. Iaea DB, Mao S, Lund FW, Maxfield FR. Role of STARD4 in sterol transport between the endocytic recycling compartment and the plasma membrane. *Mol Biol Cell*. 2017;28:1111-1122. doi:10.1091/mbc.E16-07-0499
19. Nagasaka M, Gadgeel SM. Role of chemotherapy and targeted therapy in early-stage non-small cell lung cancer. *Expert Rev Anticancer Ther*. 2018;18:63-70. doi:10.1080/14737140.2018.1409624
20. Subramaniam S, Selvaduray KR, Radhakrishnan AK. Bioactive compounds: natural defense against cancer? *Biomolecules*. 2019;9:758-772. doi:10.3390/biom9120758
21. Ma H, Zhu L, Ren J, et al. Myricetin inhibits migration and invasion of hepatocellular carcinoma MHCC97H cell line by inhibiting the EMT process. *Oncol Lett*. 2019;18:6614-6620. doi:10.3892/ol.2019.10998
22. Mohamed E, Cao Y, Rodriguez PC. Endoplasmic reticulum stress regulates tumor growth and anti-tumor immunity: a promising opportunity for cancer immunotherapy. *Cancer Immunol Immunother*. 2017;66:1069-1078. doi:10.1007/s00262-017-2019-6
23. Wang F, Song ZY, Qu XJ, et al. M10, a novel derivative of Myricetin, prevents ulcerative colitis and colorectal tumor through attenuating robust endoplasmic reticulum stress. *Carcinogenesis*. 2018;39:889-899. doi:10.1093/carcin/bgy057
24. Yang C, Lim W, Bazer FW, Song G. Myricetin suppresses invasion and promotes cell death in human placental choriocarcinoma cells through induction of oxidative stress. *Cancer Lett*. 2017;399:10-19. doi:10.1016/j.canlet.2017.04.014
25. Iurlaro R, Muñoz-Pinedo C. Cell death induced by endoplasmic reticulum stress. *FEBS J*. 2016;283:2640-2652. doi:10.1111/febs.13598
26. Sisinni L, Pietrafesa M, Lepore S, et al. Endoplasmic reticulum stress and unfolded protein response in breast cancer: the balance between apoptosis and autophagy and its role in drug resistance. *Int J Mol Sci*. 2019;20:857-873. doi:10.3390/ijms20040857
27. Li T, Su L, Lei Y, Liu X, Zhang Y, Liu X. Ddit3 and kat2a proteins regulate tnfrsf10a and tnfrsf10b expression in endoplasmic reticulum stress-mediated apoptosis in human lung cancer cells. *J Biol Chem*. 2015;290:11108-11118. doi:10.1074/jbc.M115.645333
28. Sozen E, Ozer NK. Impact of high cholesterol and endoplasmic reticulum stress on metabolic diseases: an updated mini-review. *Redox Biol*. 2017;12:456-461. doi:10.1016/j.redox.2017.02.025
29. Zhou X, Lu B, Fu D, Gui M, Yao L, Li J. Huoxue qianyang decoction ameliorates cardiac remodeling in obese spontaneously hypertensive rats in association with ATF6-CHOP endoplasmic reticulum stress signaling pathway regulation. *Biomed Pharmacother*. 2020;121:109518-109526. doi:10.1016/j.biopha.2019.109518
30. Hang L, Peng Y, Xiang R, Li X, Li Z. Ox-LDL causes endothelial cell injury through ASK1/NLRP3-mediated inflammasome activation via endoplasmic reticulum stress. *Drug Des Dev Ther*. 2020;14:731-744. doi:10.2147/dddt.S231916

SUPPORTING INFORMATION

Additional supporting information may be found in the online version of the article at the publisher's website.

How to cite this article: Li M, Zha G, Chen R, Chen X, Sun Q, Jiang H. Anticancer effects of myricetin derivatives in non-small cell lung cancer in vitro and in vivo. *Pharmacol Res Perspect*. 2022;10:e00905. doi:10.1002/prp2.905